



Project No. R19513P
Date: May 17, 2023
Humboldt, Saskatchewan

Pneumatic Grain Conveying in Seeding Equipment

TECHNICAL REPORT

Submitted To: Manitoba Crop Alliance
Carmen, Manitoba

Saskatchewan Wheat Development Commission
Saskatoon, Saskatchewan

Submitted By: Samuel Ferré, P.Eng. M.Sc.
Engineer

A handwritten signature in black ink, appearing to read "Samuel Ferré", written over a horizontal line.

Ian Paulson, P.Eng. M.Sc.
Technical Services Lead

A handwritten signature in blue ink, appearing to read "Ian Paulson", written over a horizontal line.

Charley Sprenger, B.E., M.Sc.
Project Leader

A handwritten signature in black ink, appearing to read "Charley Sprenger", written over a horizontal line.

TABLE OF CONTENTS

	Page
1. Executive Summary	1
2. Introduction	4
3. Literature review.....	6
3.1 Experimental Pneumatic Conveying Research.....	6
3.2 Simulation of Pneumatic Conveying Systems	10
4. Simulation of pneumatic conveying systems.....	13
4.1 Air-Only Model Development.....	13
4.2 CFD-DEM Model Development for Wheat Pneumatic Conveying	17
5. Results and Discussion.....	21
5.1 Two-Way Couple CFD-DEM Model Validation	22
5.2 Impact of 90° Bend on Steady State Flow Conditions	22
5.3 Pneumatic Wheat Conveying in Distributor	24
6. Conclusion	31
7. Impact on Operational Practices for Producers.....	32
8. References.....	33

ACKNOWLEDGEMENTS

This Project was made possible by funding from Manitoba Crop Alliance and the Saskatchewan Wheat Development Commission. The wheat-specific research was added as an extension to a canola research program initiated through funding by the Governments of Manitoba and Canada through the Canadian Agricultural Partnership, as well as through contributions from the Saskatchewan Canola Development Commission.

Additionally, the authors would like to acknowledge the efforts and contributions of the M.Sc. student involved with the project, Sarita Victoria Casas Urrunaga, supervising faculty Professors, Donald Bergstrom and Scott Noble, and the Mechanical Engineering Department at the University of Saskatchewan through the use of the Air Handling Laboratory.

1. EXECUTIVE SUMMARY

Air drills continue to be a popular choice for seeding many of the crops grown in the prairies today. Air drill development has continued since their invention in the 1980s, but the core of many modern air drills, the pneumatic conveying system, still relies on the passive division of seed through well-mixed, two-phase (gas-solid) flows.

Many factors are known to influence the distribution consistency of passive solid-gas flow division. In the context of air drills, these factors include seed type, seed rate, distributor geometry, fan speed, primary and secondary hose lengths and routings, and machine orientation while in operation. The implications of these complex system interactions were lacking discussion in the literature.

The physical testing and validation of these systems is known to be labour intensive, particularly for a full-scale machine. However, advancements in modern computing capacity and available simulation tools have put the investigation of these systems and the development of operational best practices by means of numerical modeling methods within reach of the industry.

Specifically, computational fluid dynamics (CFD) modeling has been used in the literature to simulate the behaviour of fluid flowing in pipes and hoses, including some published applications to agricultural pneumatic conveying. The discrete element method (DEM) is a computation method for simulating the movement and behaviour of individual (discrete) particles in granular flows. Recent developments in computational coupling schemes now enable one to simulate the response of granular particles in the presence of dynamic fluid flow fields.

To complement the previous work done for the canola conveying (Paulson, et al. [2023]), a CFD-DEM wheat model was developed to further investigate air drill primary and secondary hose routings.

The three objectives of the pneumatic wheat conveying project were to

- develop a numerical CFD-DEM model to track machine-seed interactions for wheat,
- determine the effect of air velocity, secondary hose length, and primary hose bends on the seed distribution coefficient of variance (CV) of wheat in a pneumatic conveying system, and
- recommend general routing practices for air drill manufacturers and operators to optimize wheat distribution.

Simulating the pneumatic conveying of wheat through an air drill began with the development of an air-only CFD model of a primary hose and eventually a distributor and secondary hoses. A multi-sphere wheat kernel from Petingco (2020) with a 2.4 aspect ratio was used in the two-way CFD-DEM model. The Holzer-Sommerfeld drag model and Saffman-Magnus lift model were implemented.

Four sets of wheat conveying configurations were simulated using the two-way coupled model:

- 90° bends of primary hose at three varying radii (0.64, 0.94, and 1.24 m [2.01, 3.08, and 4.1 ft]) and one fan speed (2,800 RPM).
- 9-Port idealized distributor with equal secondary hoses at three different fan speeds (2,800, 3,100, and 3,400 RPM).
- 9-Port idealized distributor with un-even secondary hoses at three different fan speeds (2,800, 3,100, and 3,400 RPM).
- 90° bend (0.94 m) primary hose into 9-Port idealized distributor with equal secondary hoses at three different offsets (0, 1, and 2 m [0, 3.28, and 6.56 ft]) and one fan speed (3,100 RPM).

A primary hose diameter of 63.5 mm (2.5 in) and single-product rate of 60.14 g/s (60 lb/ac equivalent) of wheat was used in all the simulation runs. The distributor and primary line geometry was modelled after a John Deere Air Drill (1870 Hoe Drill and 1910 Air Cart).

The modeled 90° bends demonstrated varying levels of wheat product behaviour when exiting the curved portion of the primary line. The 1.24 m (4.07 ft) radius bend had the greatest delay in product reacceleration and repositioning to prebend location near the bottom half of the pipe. The 0.64 m and 0.94 m (2.01 and 3.08 ft) bends regained their prebend conditions more quickly with less product disturbance when exiting the curvature.

Increasing the fan speed with the 9-port idealized distributor with equal secondary hoses had a detrimental effect to the CV by increasing its value proportionally. For the given product rate of wheat 60.14 g/s equivalent (60 lb/ac), a lower fan speed was more appropriate for optimizing the distribution. A recommended fan speed between 2,800 RPM and 3,500 RPM for 50 to 100 lb/ac of wheat (JD operator's manual - 1870 drill and 1910 air cart) also confirms that the lower range of fan speed would be appropriate for the simulated product rate.

Secondary runs 5 and 6 had the greatest proportion of product for all fan speeds. An equivalent 1 m (3.28 ft) of secondary hose length was added for the un-even distributor simulations. This added length was intended to create a higher restriction for the preferential lines and improve the overall distribution. The airflow was notably more imbalanced with this adjustment while the product CV change was less apparent (1% reduction in CV). Wheat seeds, being a heavier product, were less impacted by the airflow imbalance.

The offset distances from the single 90° bend (0.94 m [3.08 ft] radius) had varying impacts on the 9-port idealized distributor with equal secondary hoses. With no offset (0 m), the distributor's CV was substantially higher than the other offsets; preferential product flow towards secondary run #7 took place. The 2 m (6.5 ft) offset allowed the wheat particles time to regain their prebend position in the primary line and consistently enter the J-tube like the previous distributor configurations. The 1 m (3.28 ft) offset did not completely allow wheat product to return to its steady-state condition. Despite this, the product was impacting the J-tube in an advantageous

way that promoted more mixing and randomizing before exiting the secondary lines; this configuration had the best CV value of all simulations. It was observed that wheat particle position and velocity influenced the distributor CV.

From the simulated configurations and conditions, distribution consistency can be impacted by the following input factors: metering rate, product type, fan speed, bend radius, and distributor offset. Correctly adjusting primary and secondary hose routings to minimize the CV can be a complex endeavor with inconsistent results with varying product types and rates. What may work with one configuration may not be ideal for another. Producers should follow manufacturer recommendations for initially setting fan speeds. If seed distribution consistency is in doubt, verifying the actual performance of a drill in a static test is also recommended for finer adjustments of the fan speed and distributor configuration.

This project represented a multi-year effort in measuring air drill distribution performance, both in the laboratory and at full scale, in addition to simulating various configurations of pneumatic conveying systems. While several themes from the results point to opportunities for improved design of these systems, within the confines of existing machines, the project ultimately highlighted the importance of simple but careful maintenance of air drill pneumatic conveying components and systems.

2. INTRODUCTION

Initially developed in western Canada in the 1980s, air drills continue to be a popular choice for seeding many of the crops grown in Manitoba and Saskatchewan today. Air drill engineering development has continued since their introduction to the region, with modern air drills employing sectional control, turn compensation, variable rate control, blockage monitoring, independent row units, down-pressure adjustment features, and many other manufacturer-specific enhancements. However, the core of many modern air drills, the pneumatic conveying system, still relies on the passive division of input products (i.e., seed, fertilizer) through a well-mixed two-phase (gas-solid) flow.

Many factors are known to influence the main performance metric, distribution consistency, of passive solid-gas flow division. In the context of air drills, these factors potentially include distributor geometry and orientation, fan speed, primary and secondary hose lengths and their routings, and machine/component spatial orientations while operating in the field. Some of these factors have been studied in the open literature, but the discussion of their impact in the context of a full-scale air drill is less prevalent. The operational implications of these complex system interactions are also lacking in the literature.

The physical testing and validation of these systems is known to be labour intensive, particularly for a full-scale machine. However, advancements in modern computing capacity and available simulation tools have put the investigation of these systems and the development of operational best practices by means of numerical modeling methods within reach of the industry. Specifically, computational fluid dynamics (CFD) modeling has been used in the literature to simulate the behaviour of fluid flowing in pipes and hoses, including some published applications to agricultural pneumatic conveying. The discrete element method (DEM) is a computation method for simulating the movement and behaviour of individual (discrete) particles in granular flows. Recent developments in computational coupling schemes now enable one to simulate the response of granular particles in the presence of fluid flow fields.

To complement the previous work done by Paulson et al. (2023) with canola conveying, a CFD-DEM wheat model was developed as a tool to further investigate air drill primary and secondary hose routings.

The three objectives of the pneumatic wheat conveying project were to

- develop a numerical CFD-DEM model to track machine-seed interactions for wheat,
- determine the effect of air velocity, secondary hose length, and primary hose bends on the seed distribution coefficient of variance (CV) of wheat in a pneumatic conveying system, and
- recommend general routing practices for air drill manufacturers and operators to optimize wheat distribution.

With these objectives in mind, a review of the research literature related to experimental testing and numerical modeling of pneumatic conveying research is presented in **Section 3**. The development of the numerical model to predict both the airflow behaviour and the seed distribution performance of several configurations of pneumatic conveying systems is presented in **Section 4**. The simulation results are discussed in detail in **Section 5** and **Section 6**. Finally in **Section 7**, the impact of operational practices learned from the results of the project are discussed.

3. LITERATURE REVIEW

Existing literature was reviewed in regard to air seeder configurations and functionality, experimental pneumatic conveying research, and numerical modeling related to pneumatic conveying.

3.1 Experimental Pneumatic Conveying Research

The transportation of solid particles via a pressurized fluid media, commonly referred to as pneumatic conveying, is a method commonly used in many industries. A wide range of products can be conveyed using this approach, from fine powders (Ratnayake, 2017) to large seeds associated with agricultural air seeders, such as chickpeas. Pneumatic conveying systems are typically characterized by the operating pressure regime (positive or negative) and the solid loading ratio, which is the ratio of solid particle mass flow rate to the gas mass flow rate (Mills, 2016). Klinzing, Rizk, Marcus, and Leung (2010) define a dense phase as having a solid loading ratio greater than 15. Loading ratios less than this are called dilute phase. Most industrial pneumatic conveying systems operate in the dilute phase, including those of agricultural air seeders, thus, dilute phase pneumatic conveying was the focus of this literature review.

A consistent solids mass flow rate to all delivery points on the air drill (openers) through time is an important performance metric of modern air drill pneumatic conveying systems. Many manufacturers use a Type B pneumatic conveyance system (Allam and Wiens, 1982) with two stages: seed and/or fertilizer (generally referred to herein as product) is mechanically metered into individual *primary* air hoses/tubes. An example is shown in **Figure 1**. These meters are located on the air cart, which also includes the product storage tanks. Primary tubes are typically constructed of metal on the air cart, and then transition into flexible hose where the cart and air drill connect. Depending on the air cart manufacturer, a manual or semi-automated procedure is used to calibrate a relationship between metering roll rotations and product mass.

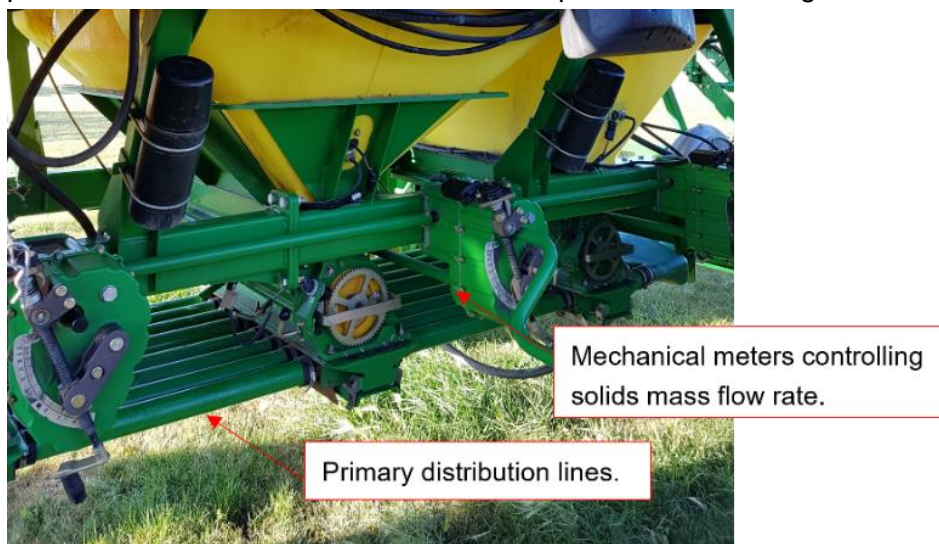


Figure 1. Primary meters controlling mass flow rate of solid product into primary distribution hoses.

Primary hoses convey the product to a secondary manifold that further divides the product and air streams into numerous secondary hoses; these secondary hoses terminate at the hoe openers of the air drill. The number of primary hoses varies, typically between 5 and 7. Secondary manifolds typically have between 6 and 12 secondary hose outlets. Secondary manifolds and hoses are shown in **Figure 2**.



Figure 2. Secondary manifolds located on the air drill frame. The division of product and air occurs passively in the secondary manifold.

Many manufacturers use a steel, J-shaped tube to transition from the nominally horizontal flexible primary hose to the distributor body, which are commonly supplied from the underside. This J-tube is evident in **Figure 3**.



Figure 3. J-tube transitioning from nominally horizontal flexible secondary hose to the secondary distributor which is fed from the underside.

Modern features, such as sectional control, turn compensation, and variable rate application are achieved by individually varying the meters that feed product into the primary hoses, typically

via an electronic control system. However, the division of product in the distributor into the secondary hoses is achieved only through the passive division of the air/product streams. The source of air flow to the pneumatic conveying system is typically one centrifugal fan (typically hydraulically driven) located upstream of the metering system on the air cart. All primary hoses are connected via a common plenum to the centrifugal fan, shown in **Figure 4**.

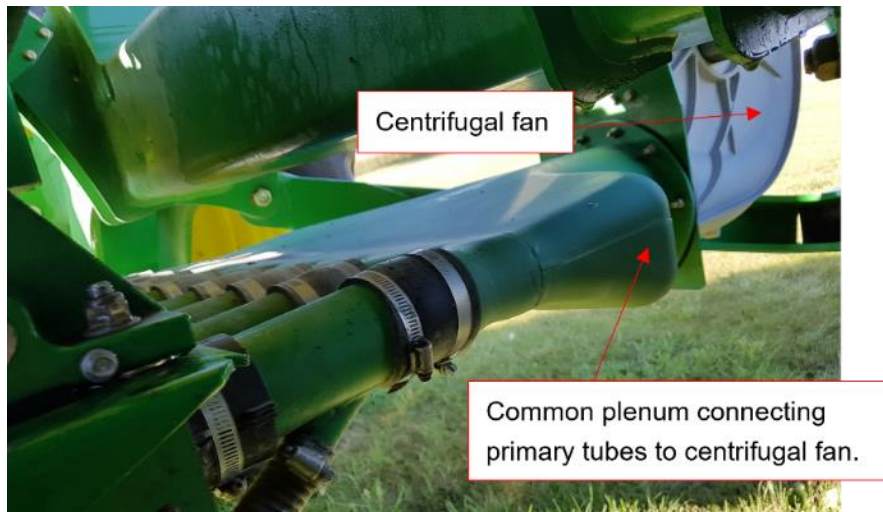


Figure 4. A centrifugal fan, the air flow source for the pneumatic conveying system, connected to primary tubes via a common plenum.

Air carts operate in an open-loop sense; that is, a feedback system is not present to confirm or maintain a constant solids mass flow rate in either the primary or secondary hoses. This has two major implications to the operator:

1. Consistency of the solids mass flow rates in the secondary hoses cannot be guaranteed.
2. An additional monitoring system is required to ensure that primary or secondary hoses have not plugged due to the accumulation of product.

To predict the solids mass flow rate in an air seeder line Hossain (2014) developed two semi-empirical mathematical models applicable to dilute phase horizontal pneumatic conveying. Measurement inputs to the models were pressure gradient and average air velocity. One model focused on the transient region 0.3 m to 0.9 m downstream of the product meters when wheat was being metered. The second model, applicable to any product, involves an on-machine parameter estimation procedure when the air drill is in use to correlate model parameters.

To further understand the flow conditions prior to plugging when conveying wheat, (Mittal, 2016) conducted extensive laboratory testing to develop the state diagram (a plot of pressure gradient versus air speed) for various solids mass flow rates of wheat conveyed through straight and bend sections of hose of similar diameter of typical primary hose. Distributor and secondary hose components were not part of the apparatus. For a given system configuration (hose length, bend radii, etc.), the pressure gradient increased with increased solids mass flow rate for a fixed air speed; a generic state diagram is shown in **Figure 5**.

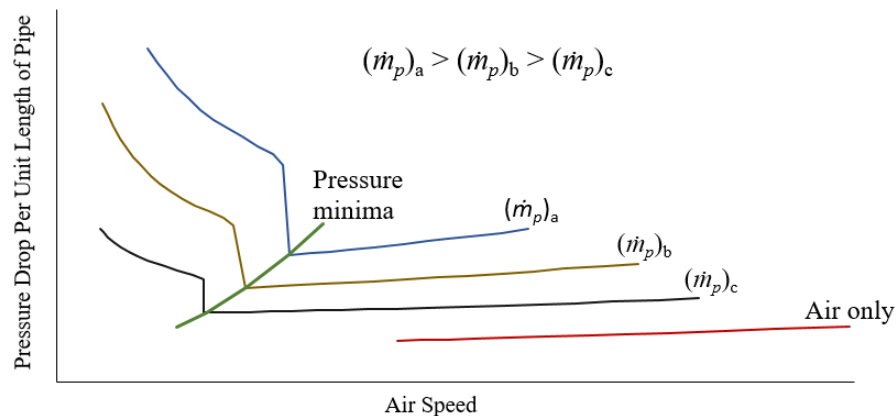


Figure 5. Generic state diagram plotting pressure drop against air speed for different solids mass flow rates. Reproduced with permission (Mittal, 2016).

As air speed was decreased, pressure gradient decreased to a minimum value; below this minimum critical speed, the pressure gradient increased sharply. Near the critical speed, product saltation was observed: grain began to settle out of the air stream and bounce and roll along the bottom of the tube (Mittal, 2016). Hubert and Kalman (2003) compared several published analytical relationships between saltation velocity and solids loading ratio. The critical speed is typically viewed as the threshold of dense phase conveyance; plugging would eventually occur if the airspeed was reduced further. As the flow transitions to dense flow, pulsing of the product occurs (Keep, 2016) which results in an inconsistent solids mass flow rate and unsteady operation of the pneumatic conveying system. These are undesirable effects for the pneumatic conveying system of an air seeder as passive product division in secondary manifolds typically relies on the solids being properly suspended in the airflow.

Practically, operators typically set the fan speed to maintain the air speed in primary hoses well above the minimum airspeed required to convey the product to decrease the risk of plugging. Susceptibility to damage from pneumatic conveying is dependent on seed type: Grieger (2018) found that germination of soybeans depended to some effect on conveyance airspeed, and it was strongly influenced by seed moisture content. Chung (1969) reported measurable damage to yellow corn based on air speed and conveyance distance. In an assessment of two different system manufacturers, vigor reduction in canola from conveyance was estimated to be between 5% and 10% depending on the variety of canola and equipment manufacturer (Bjarnason, Stock, Hultgreen, and Wassermann, 2005).

In field trials, Yatskul, Lemièrre, and Cointault (2017) found that the orientation of the primary hoses upstream of the secondary manifold affected the coefficient of variation of the distributor. Further laboratory experiments on a distributor with 20 outlets highlighted performance trends under several operating scenarios when conveying wheat. When individual outlets of the distributor were closed, an increase in the solids mass flow rate occurred not in the outlets immediately adjacent the closed secondary outlet, but in the outlets further from the closure. An increase in static pressure at the plug face was noted, and seeds were observed to first move toward the plugged outlet, then be redirected by the airflow after bouncing off the outlet plug.

Biased seed flow toward outlets not immediately beside the plugged outlet was theorized to be a result of the angular distance between outlets (dependent on design geometry).

The effect of secondary relative hose length was also tested. One secondary hose was adjusted to be longer or shorter than a standard set-up. Long hoses trended toward behaving like a blocked outlet. The solids mass flow rate of a shorter secondary hose was higher than the standard-length hoses. If an acceptable CV of 5% is assumed, the recommended relative hose length was between 0.8 and 2.5 of the standard hose length (Yatskul, Lemiere, and Cointault, 2017). Only one secondary hose (of 20) was modified in the experiment.

The geometry of the vertical pipe leading to the distributor affected the distribution uniformity. The vertical orientation and the length of the pipe were investigated. The distributor was rotated about the axis of the primary hose. The CV of distributors with smooth vertical steel pipes was more negatively impacted than distributors with corrugated/dimpled vertical pipes. Distributors with shorter tubes also had lower uniformity, with seed flow greater in the outlets that aligned with the primary hose. The authors recommended J-tube heights greater than 1.2 m (Yatskul, Lemiere, and Cointault, 2017). The introduction of a cone to the center of the underside of the distributor access lid was found to decrease the distribution uniformity. Considering the sensitivity to vertical tube height, the authors highlighted the complexity of collisions in the elbow that transitions from the horizontal primary hose to the manifold tube. Kinetic equations were presented, but this single-kernel model was not verified as part of the experimental procedure.

Kumar and Durairaj (2000) presented an experimental investigation of the impact of distributor geometry on the performance of air drills. Three different distributor geometries were considered along with the input air velocity (four levels) and seed feed rates (four levels). They highlighted a significant impact of the manifold geometry on the air velocity at the outlets of the distributor. Two important observations made by Kumar and Durairaj were (1) one of the distributors exhibited threshold values of seed feed rate and input air velocity under which uniformity of seed distribution was poor, and (2) after the threshold value, the dependency between uniformity and seed feed rate remained strong. This was a very good study that provided statistically analyzed experimental results. It, however, did not consider factors downstream of the distributor (primarily tube length and routing) nor the operational implications at the system level.

3.2 Simulation of Pneumatic Conveying Systems

The complexity of pneumatically conveying grain is evident from the experimental research presented. Product type, solids mass flow rate, conveying airspeed, and details of the system geometry are but some of the factors that affect that state of the system and subsequently the distribution uniformity. The ability to experimentally quantify system performance under so many conditions is daunting if not futile. Several researchers have developed numerical models of

various aspects of the pneumatic conveying systems of air seeders to further understand performance features.

Bourges et al. (2008) performed a computational fluid dynamics (CFD) analysis of the results presented by (Kumar and Durairaj, 2000). Bourges & Medina (2013) numerically studied a commercial secondary manifold using a weak coupling approach where the solid phase (product) is affected by the fluid phase, but the particles have no effect on the air velocity. The Lagrangian-Eulerian method was used to track the discrete solid particles in the simulation. Their results matched anecdotal evidence on the irregular distribution out of the distributor. The authors suggested the need to include the coefficient of restitution of the seeds to represent seed collisions more accurately. Here again, the authors did not elaborate on the implications of the observed behaviours on the performance of the overall system.

Cousins and Noble (2017) developed a 1-D CFD model intended for real-time control applications on an air seeder. A two-fluid (Eulerian-Eulerian) approach was used to model a straight section of air seeder primary hose. Fluid pressure predictions were found to be in good agreement with experimental data; however, solids velocities were not as accurately predicted. Improvements to model features, such as drag force estimation, were suggested. Because of the 1-D nature, particle-wall and particle-particle collisions were not represented explicitly; axial momentum loss was represented parametrically from the approach of (Eskin, Leonenko, and Vinogradov, 2007), which includes the coefficient of restitution. Considering the interest in understanding impacts between the seed and the pneumatic system geometry, a two-fluid approach is not appropriate for this project.

Bourges and Medina (2015) later investigated three different configurations of the outlets of a distributor and included the coefficient of restitution when modeling particle impacts. They observed non-uniform distribution but did not offer analysis of the observed flow patterns. In subsequent work (Bourges, Eliach, and Medina, 2017), CFD simulations of the distributor with soybeans and amaranth particles were presented. The realizable $k-\epsilon$ turbulence model was used, along with sphere-shaped particles of uniform size for a given seed type. Elastic particle-boundary collisions were represented. Solids mass flow rates at the distributor outlets were not consistent: the uniformity of soybeans was lower than the amaranth, and the patterns were not consistent with air flow patterns. The lower outlet variation of amaranth was attributed to it having a lower Stokes number than soybeans. System-level observations were not provided.

In a white paper from Bayati and Johnston (2017), two modeling approaches were presented, with a focus on variance of the solids mass flow rate in secondary hoses through time. Both wheat and soybeans were modeled: one-way coupling was used in the wheat simulations, due to its low momentum coupling factor; soybean-air interactions were modeled using two-way coupling where the particles and air affect each other as the momentum coupling factor was an order of magnitude larger than that of wheat. The standard $k-\epsilon$ turbulence model was used, along with the Lagrangian method to track particle motion within an Eulerian representation of

the fluid. The larger soybean particles tended to cluster (high solids mass flow rate variance through time at the manifold outlets). Both particle types tended to stagnate in the manifold until adequate pressure was developed to carry the seeds down the secondary hoses.

Ebrahimi (2014) provided a road map for developing and experimentally validating a CFD-DEM pneumatic conveying model using both spherical glass beads (0.9 mm, 1.5 mm, and 2.0 mm mean diameters) and cylindrical polyamide6 particles (1 mm x 1.5 mm). Particle and air velocity were measured using laser Doppler anemometry. Measured velocity profiles through both vertical and horizontal cross sections at multiple solids loading ratios and at multiple distances downstream of the injection point were reported for both the carrier fluid (air) and the particles in the experiments involving both particle types. Similarly, the turbulence intensity profiles of the carrier fluid from the experiments were reported.

Additionally, Ebrahimi (2014) evaluated the influence of the Magnus lift force on spherical particles in the coupled CFD-DEM model by comparing its contribution compared to gravitational and drag forces as well as considering the number of particles that were carried in the upper portion of the pipeline cross-section (i.e., the probability distribution of the vertical position of seeds; additional experimental results of this quantity for conveying wheat are provided in Keep (2016). The Magnus lift force model was included in subsequent simulations (Ebrahimi, 2014). For cylindrical particles, the effect of the Ganser (1993), and Haider and Levenspiel (1989) drag models were investigated. Both of these models are available as particle body forces in EDEM (Altair Engineering Inc., 2021) discrete element method software, which will be used as the DEM simulation engine for this project.

Boac et al. (2010) compiled a comprehensive list of physical parameters for a variety of seed types from the literature, including canola and wheat; however, the coefficient of restitution for boundary collisions was not reported.

Petingco (2020) evaluated 7 different varieties of Hard Red Winter Wheat with respect to size distribution and bulk density packing. The physical shape, contact parameters, and distribution of DEM particles (sphere based) were investigated. Optimized parameters of the particles for bulk density are proposed with a validated model. The simplified wheat kernel was selected for the CFD-DEM model of this project.

4. SIMULATION OF PNEUMATIC CONVEYING SYSTEMS

Prior simulation and experimental work in the literature, along with the single-hose lab testing and full-scale machine testing, was used as a foundation to develop several scenarios of first an “air-only” numerical model (no seed introduced), followed by models of wheat being pneumatically conveyed. The development of these models is discussed.

4.1 Air-Only Model Development

Experimental work to measure pressure gradients from Mittal (2016), along with the combination of experiments and simulations from Ebrahimi (2014) that described the velocity profile of air in round ducts, provided a foundation for the development of the air-only CFD model for the primary hoses of the pneumatic conveying system. Reynolds number (Re_D) is a dimensionless fluid velocity used throughout fluid mechanics to characterize a flow (**Eq [4]**):

$$Re_D = \frac{\rho \bar{V} D}{\mu} \quad [4]$$

where ρ is the density of the fluid (air), \bar{V} is the average velocity of the fluid in the pipe, D is the diameter of the pipe and μ is the viscosity of the fluid.

Additionally, the power law of the velocity profile in a round duct provided an empirical description of velocity as a function of radial position. Specifically, **Eq [5]**:

$$\frac{V}{V_{max}} = \left(1 - \frac{r}{R}\right)^{1/n} \quad [5]$$

where V is the velocity at radial position r , V_{max} is the maximum velocity at the centerline of the pipe, R is the radius of the pipe, and n is an empirical constant taken as 7.0 for turbulent flows.

The average and maximum velocity in the pipe were related through **Eq [6]** and **Eq [7]** (White, 2006):

$$f = 0.316 Re_D^{-0.25} \quad [6]$$

and

$$\frac{\bar{V}}{V_{max}} = (1 + 1.3\sqrt{f})^{-1} \quad [7]$$

where f is the Darcy friction factor, where a smooth wall was assumed throughout this work.

Also worth noting is the relationship between the volumetric flow rate, Q , and pressure drop per unit length $\frac{\Delta p}{L}$, given in **Eq [8]** (White, 2006):

$$Q = \frac{1}{4}\pi D^2 \bar{V}$$

[8]

$$\frac{\Delta p}{L} \approx 0.241 \rho^{3/4} \mu^{1/4} D^{-4.75} Q^{1.75}$$

The exponent of D indicates that the pressure drop predicated along a pipe is highly sensitive to its diameter, with inconsistencies and uncertainties in the pipe diameter being a potential notable source of error between measured and predicted values.

Managing the computational cost of the simulations was a consistent challenge throughout the modeling process, due to several implications:

1. Lower-cost models enable more geometry/operational configurations to be investigated for a given software license/computer asset over a fixed period of time.
2. The viability of two-way coupled CFD-DEM simulations, which would be required for heavier seeds and greater solids mass flow rates, is strongly affected by the computational cost of the CFD model, as the flow field of the fluid is recomputed at each timestep (typically hundreds of times per second of simulated time).

In CFD simulations, the fluid domain is discretized into finite volumes over which the relevant equations of momentum and mass conservation are solved numerically. These discretized volumes are referred to as the *grid*; typically, a finer grid (smaller finite volumes) permits a more accurate solution. However, more grid cells increase the computational costs to solve a given simulation (i.e., runtime, computational core count).

To capture the gradient present in the boundary layer flow against walls, the grid cells against boundaries are required to be smaller than cells located further from the wall in the rest of the flow field. However, these small cells (termed inflation layers) increase the computational cost. Using the geometry from Ebrahimi (2014), a model of a straight tube was developed to compare the impact of not using inflation layers in the grid. Meshing parameters are given in **Table 1**. The streamwise velocity profiles across the radius of the pipe (inner diameter [ID] = 0.075 m) are shown in **Figure 6**. A commercially developed CFD code, HyperWorks CFD (Altair Engineering Inc., 2021) was used throughout the project for the development and solving of the CFD results.

Table 1. Mesh parameters used to compare the impact of not using inflation layers.

Parameter	With Inflation Layers	Without Inflation Layers
Surface cell size (m)	0.005	0.005
Volume mesh size (m)	0.0075	0.0075
Minimum cell size (m)	0.001	0.004
First inflation layer cell height (m)	0.0015	-
Number of inflation layers	3	-
Total number of cells	1.37x10 ⁶	1.12x10 ⁶

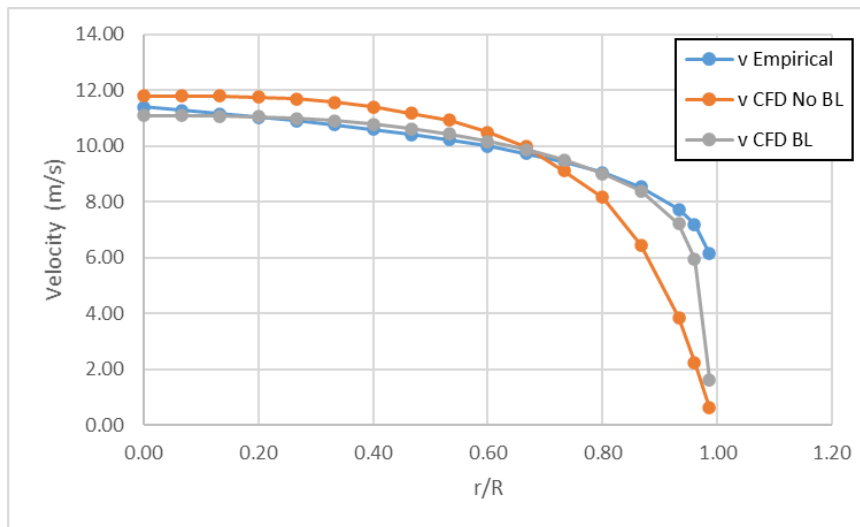


Figure 6. The streamwise velocity profile of a CFD simulation with and without inflation layer grid cells, compared to the empirical fit.

The overall agreement with the empirical solution was significantly improved with the presence of inflation layers in the grid. With inflation layers, the velocity both at the centerline of the tube ($0\ r/R$), and near the wall ($\sim 1.0\ r/R$) was more accurate. The trend in the gas velocity profiles reported by Ebrahimi (2014; not shown) indicated a slight underprediction of the velocity by the empirical power law throughout much of the profile.

The simulation was also compared to experimental pressure gradient values for air-only pneumatic systems reported in the literature (Mittal, 2016). A simplified version of the experimental apparatus used in that experimental work was developed. In the experiments, wheat was pneumatically conveyed through a 57-mm ID horizontal pipe at three grain feed rates (20, 60, and 100 g/s) using air velocities ranging from 7 to 21 m/s.

Mittal (2016) concluded that the bend-angle of the test apparatus had a negligible effect on the pressure drop when only conveying air (no particles present). As an initial check of this new model geometry, an air-only condition with a 90° bend was simulated at 15 m/s. The pressure drop in the straight section of the model was approximately 45.7 Pa/m. The estimated average pressure drop through the five bend angles tested (0.0° , 22.5° , 45.0° , 67.5° , and 90.0°) ranged between from 35 to 40 Pa/m at this airspeed. The model geometry is shown in **Figure 7**.

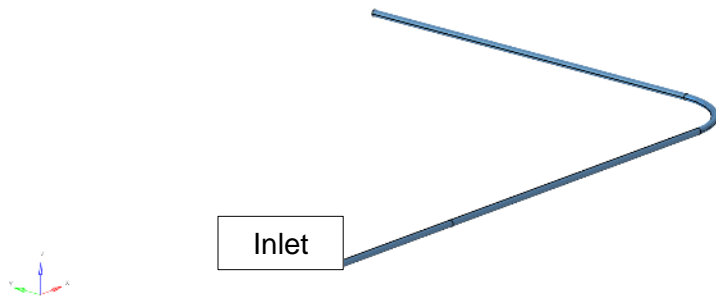


Figure 7. The geometry replicating the experimental apparatus of Mittal (2016) in the 90° bend configuration. The distance between the inlet and the start of the bend was 4.75 m. The ID of the tube was 57 mm, with the flexible elbow having an ID of 63.5 mm.

CFD grid parameters from the CFD model are listed in **Table 2**.

Table 2. CFD grid parameters for the model based on Mittal (2016) experiments.

Parameter	Value
Surface cell size (m)	0.005
Volume mesh size (m)	0.010
Minimum cell size (m)	0.00075
First inflation layer cell height (m)	0.001
Number of inflation layers	3
Number of cells	1.88x10 ⁶

Development of the CFD model then turned to the J-tube and distributor housing itself, along with the secondary hoses connected to the outlets of the distributor. The geometry was developed from measurements taken of the air cart and drill (JD 1870) used during full-scale testing (Paulson et al. (2023)); a CAD model of the simplified geometry is shown in **Figure 8**. Note that because the fluid domain is the meshed volume in CFD, the geometry in **Figure 8** is that of the air volume within the hoses and distributor and not of the physical components.

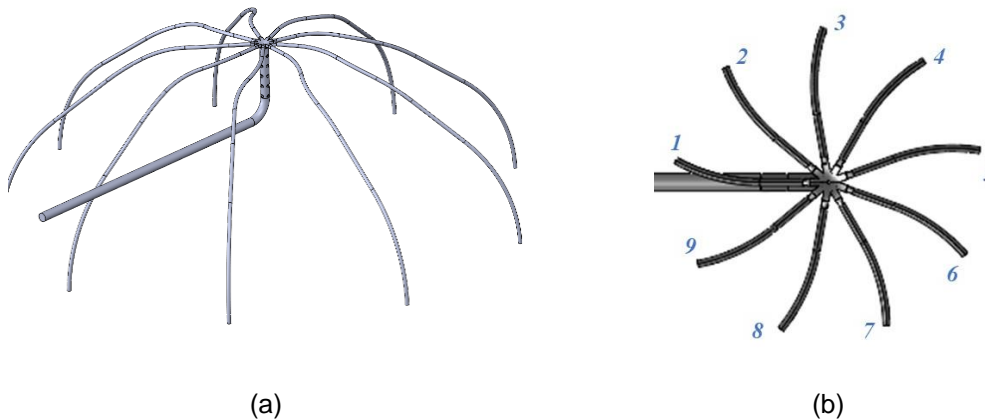


Figure 8. The CAD model of a simplified primary hose, distributor, and secondary hoses for a distributor with nine outlets, viewed isometrically (a), and from above (b).

A distributor with nine outlets was simulated throughout this work as it was the more common configuration on the drill used in full-scale testing. Secondary position 1 was directly in line with the approaching primary, with numbering proceeding clockwise as viewed from above.

4.2 CFD-DEM Model Development for Wheat Pneumatic Conveying

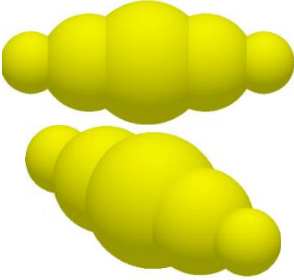
While the insights gleaned from an air-only model can be illustrative of the fundamental performance of a pneumatic conveying system, simulating the transport and distribution of solid particulate ultimately requires a representation of the solid particles to be included in the simulation of the system. Multiple solid-gas simulation approaches exist; this can range from a two-fluid model, where the solids phase is abstracted as a second fluid, to the discrete representation of each particle, including its interaction with both walls and other particles present in the model, by using the discrete element method (DEM). Discrete element method models were developed in the commercially available software EDEM (Altair Engineering Inc., 2021).

Pneumatic conveying applications in agriculture typically involve relatively large particles with non-negligible inertia that are also influenced by interactions with wall boundaries and other particles. Thus, the need to use a DEM representation of particles coupled to a CFD flow field of the gas was identified early in the project. After this, the need to simulate the flow field, model wheat using a DEM approach, and determine an appropriate means to communicate the forces between the particles and the gas became the natural tasks required to develop a pneumatic conveying model of wheat. The development of the flow field simulation was discussed in **Section 4.1**. The representation of wheat using DEM, and the coupling between DEM particles and the CFD flow field are discussed below.

Values for the physical characterization of wheat, along with DEM particle-particle and particle-wall interaction parameters were taken from the literature (Petingco, 2020). Several shapes of wheat kernels were investigated by Petingco (2020), the small kernel (2.4 aspect ratio) from set 1 was selected for the DEM model. The smaller kernel was preferable for model stability with respect to the particle volume fraction within the smaller inflation layers at the wall surfaces. The specific values used in the simulations are given in **Table 3**.

It is noted that the sensitivity of the simulation results to the particle-wall interaction parameters was not investigated during the course of this work. However, given the potential range of interaction values for varying hose materials and surface conditions produced by several vendors, the selected values below likely represent one of the many possible appropriate values for this aspect of the simulations.

Table 3. DEM parameters used in the simulation of Wheat in an air seeder (Petingco, 2020).

Parameter	Value
Particle solid density (kg/m ³)	1373
Particle Poisson's ratio	0.22
Particle shear modulus (MPa)	22.4
Particle-particle coefficient of restitution	0.5
Particle-particle coefficient of static friction	0.26
Particle-particle coefficient of rolling friction	0.01
Particle-hose coefficient of restitution	0.33
Particle-hose coefficient of static friction	0.17
Particle-hose coefficient of rolling friction	0.02
	m = 0.016 g D = 5.52 mm d = 2.32 mm Aspect Ratio = 2.4 Sphere 1: rad. = 0.581 mm pos = 2.179 mm Sphere 2: rad. = 0.914 mm pos = 1.090 mm Sphere 3: rad. = 1.160 mm pos = 0.000 mm Sphere 4: rad. = 0.914 mm pos = -1.090 mm Sphere 5: rad. = 0.581 mm pos = -2.179 mm

When coupling CFD and DEM simulations, a choice between *one-way* and *two-way* coupling for the simulation engine is required:

- One-way coupling: aerodynamic forces of the fluid flow acting on a particle are communicated to the particles during the simulation. This results in the particle being influenced by the given features of the flow field. However, the impact of the particle on the flow field (e.g., momentum transfer, turbulence modulation, mass conservation implications from particle introductions) are not included in the simulation. A static CFD solution can be solved first, and subsequently used to calculate aerodynamic forces on particles as they travel through the system.
- Two-way coupling: in addition to the aerodynamic forces being transferred onto the solid particle phase, the solid particle phase is recognized within the CFD simulation and both evolution of the fluid and particle flows develop simultaneously. The volume of individual DEM particles is accounted for in the CFD volume cells. These simulations are inherently transient.

While two-way coupling provides a more complete representation of the two-phase system, it requires the CFD and DEM models to run and solve simultaneously. This is typically orders of magnitude greater in terms of computation cost in comparison to a one-way coupled model. Due to the moderate solid loading ratio and the larger size of wheat kernels (relative to canola), two-way coupling was used throughout the modeling of the pneumatic conveying of wheat in

this work. EDEM and AcuSolve (Altair Engineering Inc., 2021) were used as the DEM and CFD simulation tools, respectively.

The flow field mesh parameters were consistent with the Air-Only model development (**Section 4.1**). Equivalent inlet conditions were based on air drill fan velocities, noted in **Table 4** along with additional model settings.

Table 4. Two-Way boundary conditions values used based on full-scale testing, and other model and mesh parameters.

Parameter	Value		
Fan speed (RPM)	2800	3100	3400
Inlet average velocity (m/s)	17.5	19.3	21.3
DEM Particle Mass Flow Rate (g/s) [lb/ac at 5 mph for 56 ft width + 6 primary runs]	60.14 g/s [60 lb/ac]		
Numerical method	Reynolds-averaged Navier Stokes (RANS)		
Turbulence Model	RANS Spalart-Allmaras		
Wall roughness	Smooth		
Drag Model	Holzer-Sommerfeld		
Lift Model	Saffman and Magnus		
First-cell heights (mm)	Primary hose and J-tube = 1.8 Distributor = 1.0 Secondary hose = 1.5		
Max. cell size (mm)	Primary hose = 5.0 J-tube = 4.0 Distributor = 2.0 Secondary hose = 2.5		
CFD Transient Time Step (s)	3.5E-04		
DEM Time Step (s)	3.5E-06		

Ebrahimi (2014) identified the importance of including the Magnus lift force when modeling the pneumatic transport of spherical particles. This lift force model, based on the angular velocity of a particle, along with the Saffman lift model and the Holzer-Sommerfeld drag force model, were used throughout the simulations to communicate the aerodynamic forces from the fluid flow field onto the particles.

The Spalart-Allmaras turbulence model was selected for its decreased complexity and reduced solver time. For this relatively simple flow domain and air velocity range, the Spalart-Allmaras was deemed appropriate for this application.

The Holzer-Sommerfeld drag model was selected for its ability to account for non-spherical (multi-sphere instead of single sphere) particle shapes and orientations. The aspect ratio and volume of the multi-sphere wheat kernel are inputs for this drag model. These features are significant advantages over other drag models that tend to simplify particles to a single larger

sphere. This simplification can lead to simulation discrepancies with respect to general particle behavior and system pressure drop.

An equivalent seeding rate of 60 lb/ac was selected since it also closely coincided with data from Mittal (2016) at 60.14 g/s in a primary line. This rate, closer to the lower range, minimized the overall particle count during the simulation runs and corresponding computational time.

4.2.1 Experimental Design for Two-Way DEM-CFD Simulations

Beyond the numerical model development initiatives, a portion of the project scope was also to evaluate the effects and implications of fan settings and general hose routings (primary and secondary) on the wheat distribution for air drills.

Depending on the manufacturer’s design, hose routings can be adjusted on air drills. Toolbar width, folding style, and row spacing often dictate how routings are configured. When adjustment is possible (from factory or at maintenance intervals), knowing how to optimize the primary and secondary hoses could result in improved product distribution. The experimental design in **Table 5** was developed to identify the distribution performance in the different primary and secondary hose configurations.

Table 5. Experimental Design for Two-Way DEM-CFD Simulations

Simulation	Dependent Variable	Independent Variable
90° Bend for Primary Hose (at 2,800 RPM)	Particle Velocity Out of the Bend	Bend Radius (0.64, 0.94, and 1.24 m)
9-Port Distributor w/ Even Secondary Hoses	Particle Distribution	Fan Speed (2,800, 3,100, and 3,400 RPM)
9-Port Distributor w/ Un-Even Secondary Hoses	Particle Distribution	Fan Speed (2,800, 3,100, and 3,400 RPM)
90° Bend into 9-Port Distributor with Even Secondary Hoses (at 3,100 RPM)	Particle Distribution	Distance from out of 90° Bend (0.00, 1.00, and 2.00 m)

The distributor and hose geometry were based on the John Deere Air Drill (1870 Hoe Drill and 1910 Air Cart) used in the physical testing (previously conducted in the pneumatic conveying of canola, **Figure 8**). The fan speeds recommendations were between 2,800 RPM and 3,500 RPM for 50 to 100 lb/ac of wheat at 5 mph (for the given air drill width [56 ft] and single shoot configuration). The inlet velocities of 17.5, 19.3, and 21.3 m/s (54.4, 63.3, 68.9 ft/s) were equivalent to 2,800 RPM, 3,100 RPM, and 3,400 RPM, respectively.

The three bend radii were approximated from what was roughly measured on different primary lines on the 1870 Hoe Drill. Product velocity into and out of the 90° bend was of interest because of the potential downstream effects on the distributor. Kumar and Durairaj (2000) had indicated an impact on distribution based on air velocity, seed rate, and geometry without studying upstream effects (i.e., primary hose routing). Investigating particle velocity and positioning leading into the distributor was the reason for simulating the 90° bends (with and without distributor, **Figure 9** and **Figure 10**).

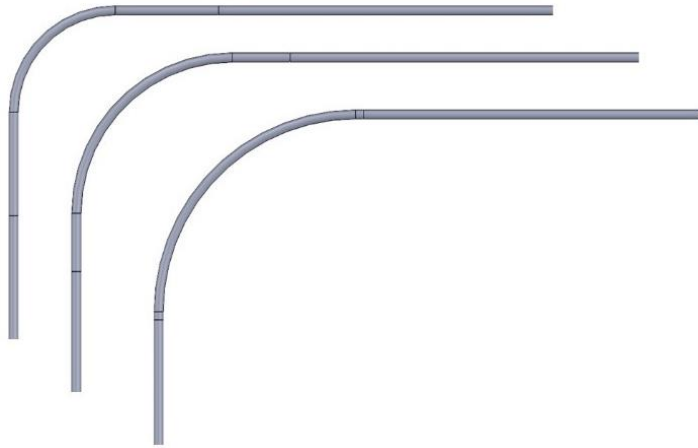


Figure 9. 90° Bend primary hose geometry (radius: 0.64 m, 0.94 m, and 1.24 m [2.01, 3.08, and 4.1 ft]), top view.

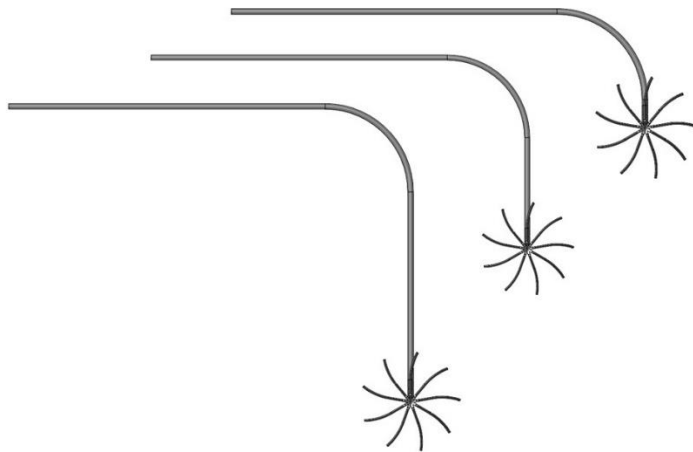


Figure 10. 90° bend into 9-port distributor (distances from bend: 0.0 m, 1.00 m, and 2.00 m [0.0, 3.28, and 6.54 ft]), top view.

5. RESULTS AND DISCUSSION

The behavior of a two-phase CFD-DEM model (with full two-way coupling) was of interest, as it was anticipated that both phases would play an important role in the distribution performance of an air drill, especially when conveying wheat. The activities and results from air-only simulations are fully presented and discussed in the previous report by Paulson et al. (2023). Knowledge from this model led to the development of both the canola and wheat conveying models. The two-way couple CFD-DEM model for wheat conveying will be the focus of the discussion in this section.

5.1 Two-Way Couple CFD-DEM Model Validation

Acceptable error values can be difficult to quantify when validating overall numerical models to physical experiments. Varying levels of error can be present for the parameter of interest. For instance, the general particle behavior (i.e., velocity, contact forces, and general flow) and airflow response (i.e., velocity, pressure drop, and flow gradient) may have varying degrees of error. In some cases, models may need to be adapted to accommodate the lowest possible error for the parameter of interest. For this project, limited data was available for the studied geometry and configurations. Static pressure drop data from Mittal (2016) wheat conveying lab experiments was used to compare and validate a portion of the developed CFD-DEM wheat model.

A horizontal straight pipe segment (L1) was replicated like the one used by Mittal (2016). Two separate operating conditions were selected for comparison: wheat 60 g/s (15 m/s) airflow and wheat 100 g/s (18 m/s) airflow. **Table 6** displays a pressure drop comparison between the experimental tests and simulation results. As shown, the error varied between 14.3% and 17.7% for the 60 and 100 g/s mering rate, respectively. The error could be further reduced with a more refined model but at a higher computational cost. Model instabilities can also be present when a volume mesh cell's volume fraction is reduced (large particle in smaller cell). It should also be noted that the wheat flow pattern (regime 2 to 3) identified by Mittal (2016) was in line with the observed numerical wheat particles. Without further experimental tests, it is difficult to completely evaluate all aspects of the two-way couple wheat model. Despite this, the current numerical model allows for a reasonable delay of computational time and stability for the level of accuracy.

Table 6. Static pressure drop and error comparison for experimental and numerical modeling.

L1 -Delta (Pa) and Error Comparison			
	Testing	Simulation	% Error
60 g/s @ 15 m/s	33.6	39.5	17.7
100 g/s @ 18 m/s	67.1	57.5	14.3

5.2 Impact of 90° Bend on Steady State Flow Conditions

A single inlet velocity of 17.5 m/s (3,100 RPM equivalent) was used to convey 60.14 g/s (60 lb/ac equivalent) of wheat in three different sizes of bends: 0.64 m, 0.94 m, and 1.24 m (2.01, 3.08, and 4.1 ft). A single diameter pipe of 63.5 mm (2.5 in) was selected. Approximately 5 m (16 ft) of pipe length was connected into and out of the bend. **Figure 11** displays an example of simulation domain with the analysis bins for wheat particles entering and leaving the bend.

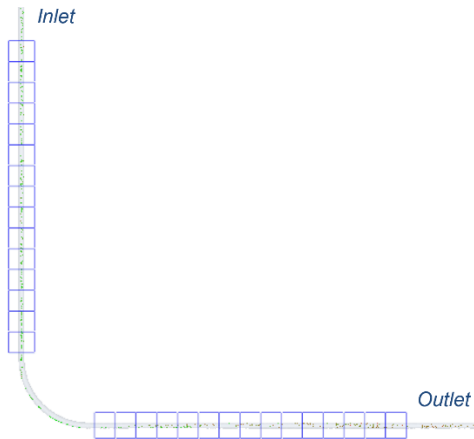


Figure 11. 90° bend simulation layout example (0.64 m [2.01 ft] radius) with analysis bins for particle entering and leaving the bend.

Figure 12 has all three 90° bends with wheat particles being conveyed at a steady state. As expected, the change in direction becomes more gradual with a larger radius bend. The interruption in the flow regime is variable and may be impacted by the product type, rate, and airflow. A larger bend radius may not always equate to a more stable flow with respect to regaining the original flow pattern (leading into a bend).



Figure 12. 90° bend simulations with velocity gradient profiles (0 to 12.5 m/s).

Figure 13 and **Figure 14** present the wheat particle velocity along the direction of travel leading into and out of the bend respectively. All three bends have a similar input velocity going into the 90° elbow. A notable behavior from **Figure 14** shows that the time required to reaccelerate is higher with the larger radius bends simulated. The 1.24 m (4.06 ft) bend is gradual enough to allow particles to accelerate through the bend causing an over correction and larger distance before centering and regaining velocity. As smoother transition and reacceleration can be seen with the 0.64 m and 0.94 m (2.01 and 3.08 ft) radius bends both in **Figure 12** and **Figure 14**.

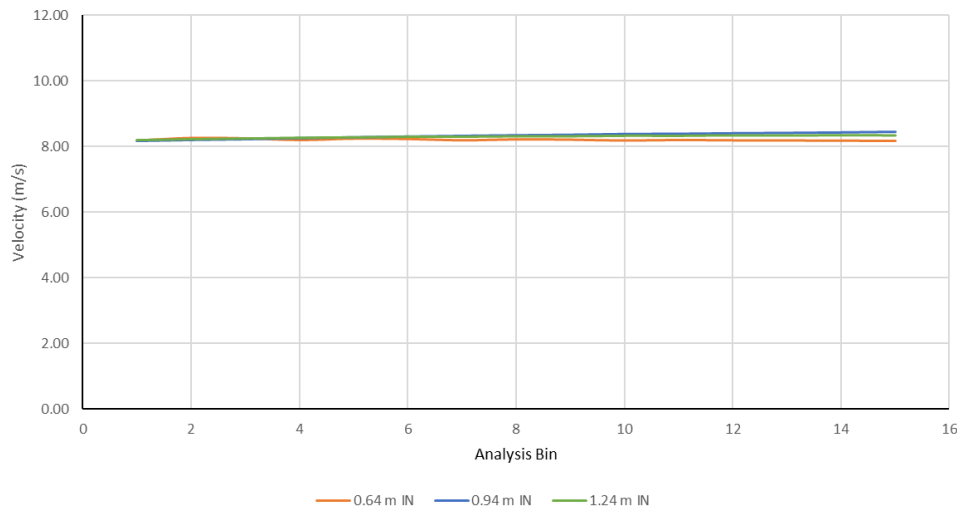


Figure 13. Particle velocity along direction of travel leading into the 90° bends (left to right – furthest to closest to bend).

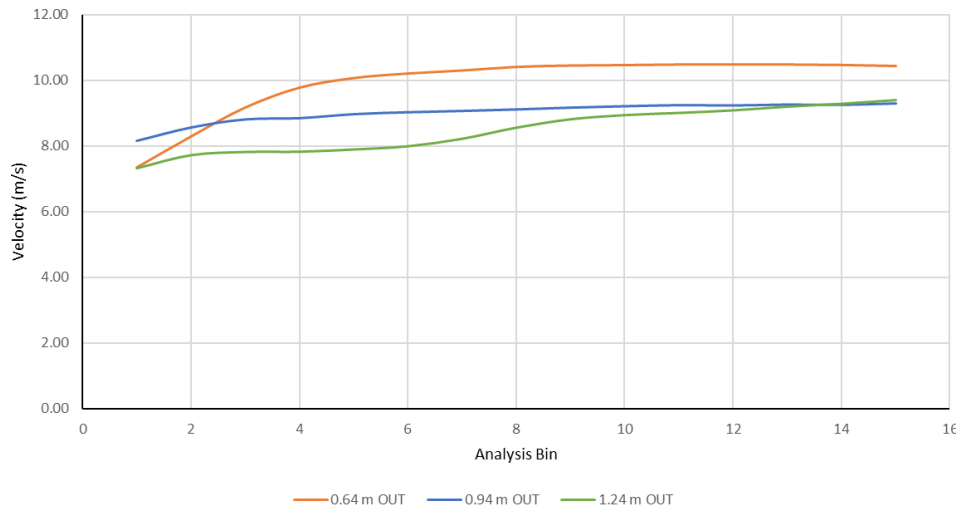


Figure 14. Particle velocity along direction of travel leaving the 90° bends (left to right – closest to furthest of bend).

5.3 Pneumatic Wheat Conveying in Distributor

Discussion regarding wheat conveying in the distributor is presented in the following subsections.

5.3.1 Impact of Secondary Hose Length and Fan Speed on Wheat Distribution

The simulations of the idealized distributor with equal length hoses are discussed first, followed by the impact of unequal length hoses. Both configurations were subjected to three fans speeds (2,800, 3,100, 3,400 RPM). A primary hose diameter of 63.5 mm (2.5 in) and single product rate of 60.14 g/s (60 lb/ac equivalent) of wheat was used in all distributor simulations. The secondary outlets are consistently identified as displayed in **Figure 15**.

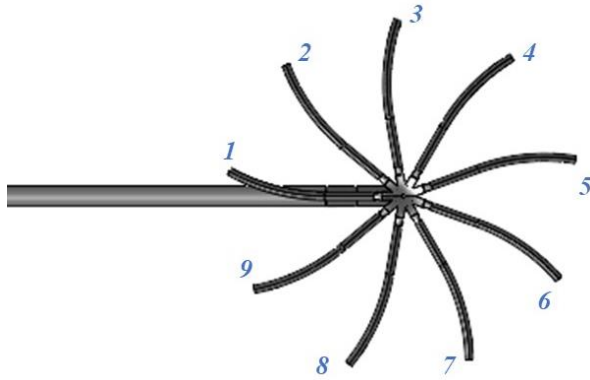


Figure 15. Secondary hose outlet labeling for all simulated distributors.

In the model shown in **Figure 8** with equal length secondary hoses, particle flow developed through approximately the first half of the primary pipe and particles tended to travel in the lower half of the pipe cross section prior to entering the J-tube, as shown in **Figure 16**. For the given mass rate entering the domain and the air velocity range, the wheat particles occupying the lower half of the primary pipe (regime 2 to 3) did coincide with the general behaviors observed by Mittal (2016). Mittal (2016) had observed a greater amount of particle suspension with increasing air velocities.

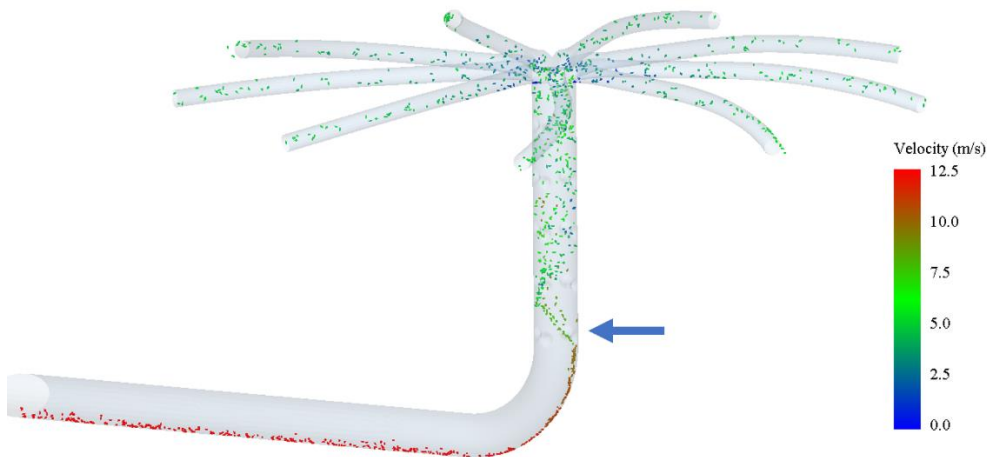


Figure 16. Wheat particle trajectory colored by velocity with the airflow based on 3,100 RPM through the system with secondary hoses of equal length (simplified geometry for visualization). The blue arrow indicated the location of the lowest dimple on the back side of the J-tube.

Most of the wheat particles impacted the outside curve of the J-tube elbow and then bounced upward and against the front side of the tube. The impact of the first dimple, identified by the blue arrow in **Figure 16**, had a significant role in deviating the wheat particle flow. As typically intended by the design, dimple tubes promote the mixing and randomization of product prior to entering the secondary hoses. With a heavier product like wheat, the natural tendency of the flow was to maintain contact closer to the outside of the J-tube bend. **Figure 17** consistently outlines the slightly higher mass fraction in outlets 5 and 6 for all three fan speeds. The coefficient of variation (CV) also trends higher with an increasing fan speed. The higher air

velocity accentuated the distribution offset to the outside of the curve and caused for a greater product imbalance for this specific distributor design.

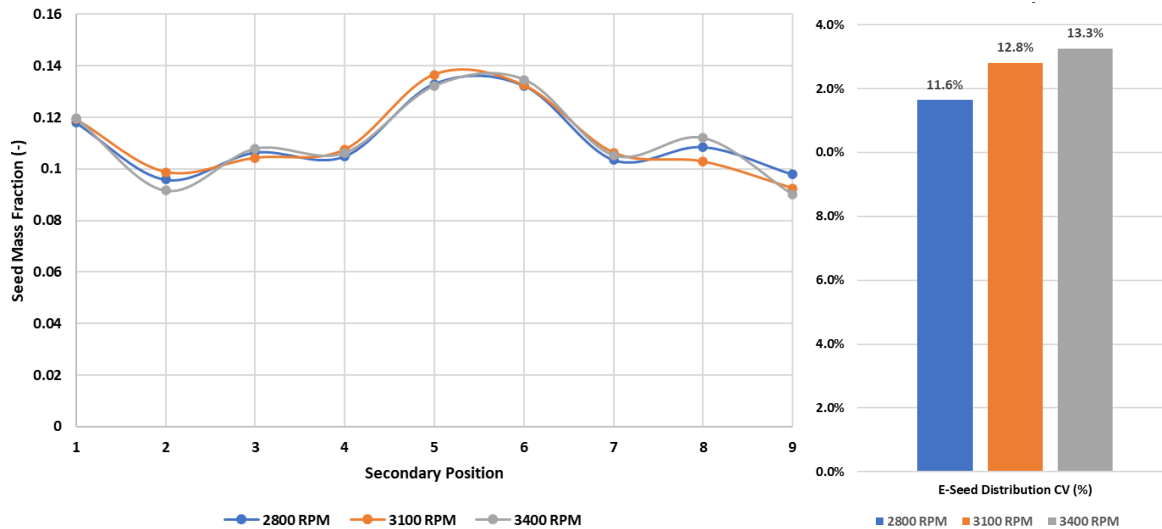


Figure 17. Wheat seed mass fraction through each secondary hose of equal length and CV during the three simulated fan speeds.

Figure 18 displays the particle average velocity leading into the J-tube distributor. As expected, increasing the fan speed results in a higher particle velocity into the distributor. Like **Figure 17** suggests, air velocity needs to be optimized with respect to product type and metering rate to ensure the best possible CV. Air drill manufacturers will typically have an approximate fan speed range for specific operating conditions. As such, selecting the exact fan speed within the range may require some additional considerations.

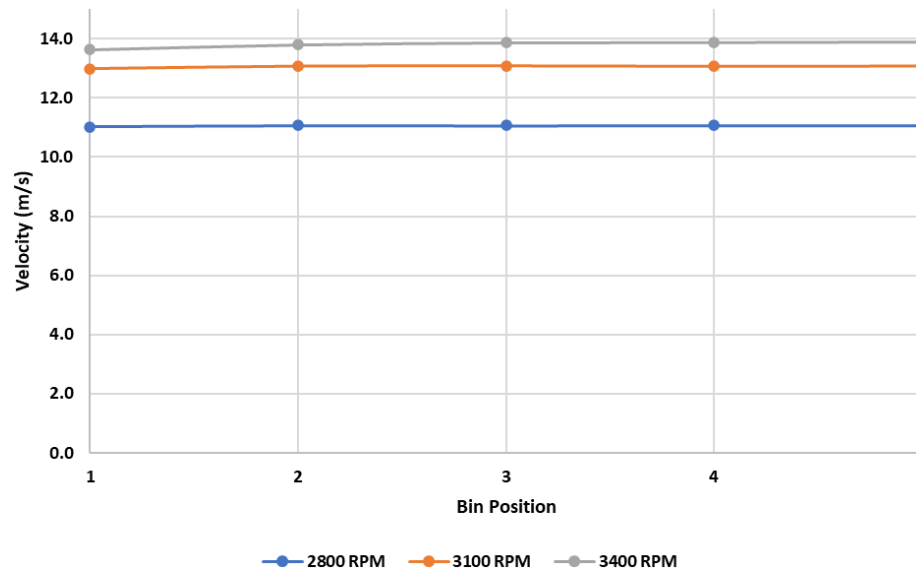


Figure 18. Particle velocity along direction entering the J-tube distributor (left to right/furthest to closest to distributor) for distributor with equal hose lengths.

Following the post processing of the equal length distributor, an equivalent 1 m (3.28 ft) of hose length was added to the two secondary runs with the higher wheat counts (5 and 6). This was

done in the effort to create a greater restriction in the favored runs (5 and 6) and balance the wheat distribution.

Figure 19 overlays the even and uneven hose length distribution results. Despite inducing a greater restriction on runs 5 and 6, a significant difference between the two configurations is difficult to identify. **Figure 20** shows the associated CV for the airflow and seed distribution for the respective fan speeds and hose configurations. The added hose length has increased the airflow CV from approximately 2% to 8%. Inversely, the seed distribution CV as slightly improved by approximately 1%. Heavier seeds like wheat may need an even greater restriction in the targeted runs to have a significant impact on the overall product CV. With respect to increasing the secondary hose lengths, this may become impractical by the time a lower CV is attained. Adjusting hose lengths will have a greater impact on the CV with lighter seeds such as canola that tend to be more influenced by the airflow (Paulson et al. [2023]).

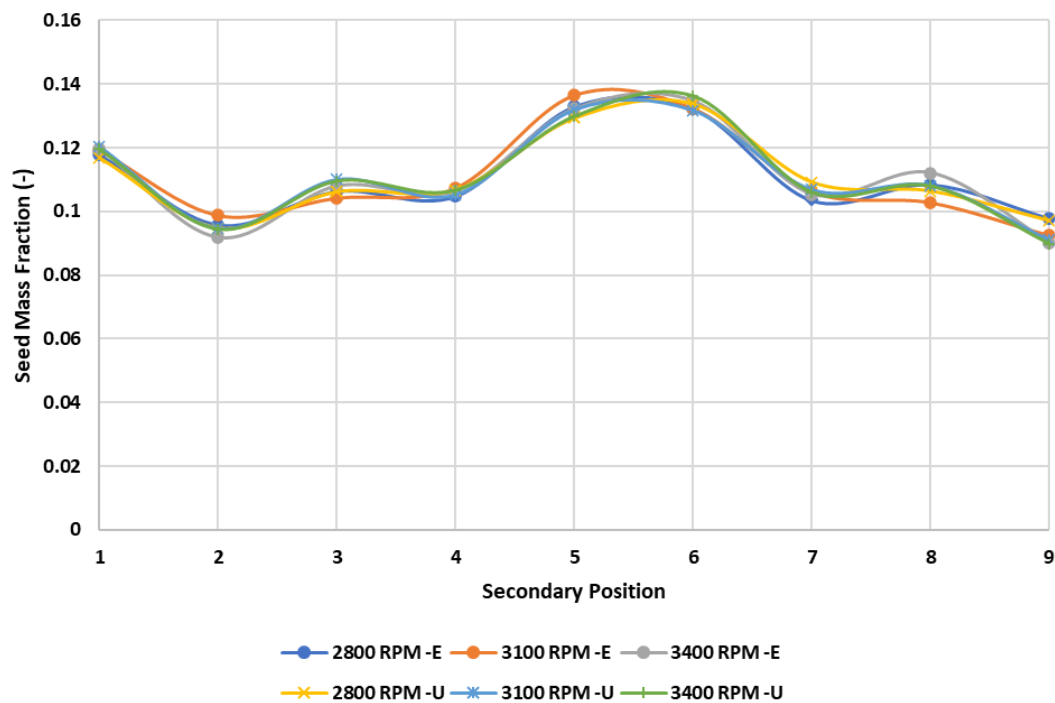


Figure 19. Wheat seed mass fraction through each secondary hose of even (E) and uneven (U) lengths, during the three fan speeds simulated.

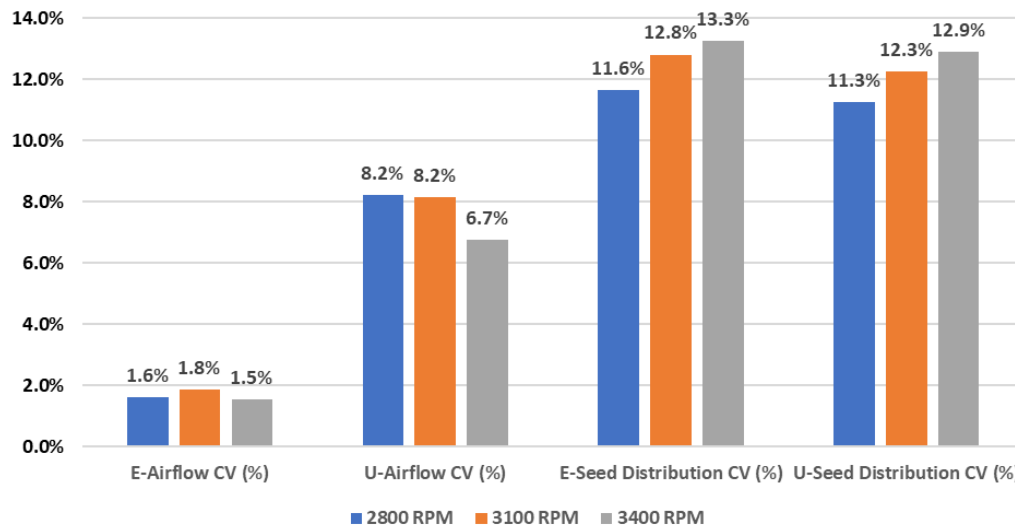


Figure 20. The airflow and seed coefficients of variation for even (E) and uneven (U) hose lengths at three different fan speeds.

5.3.2 Impact of Upstream Primary Hose Routing on Wheat Distribution

Based on the previous work done by Paulson et al. (2023), the full-scale simulations and tests (primary runs with distributors) identified a significant impact on airflow distribution from the upstream hose routings (i.e, bends, dips, and straight segments). This portion of the project was intended to quantify the effect of positioning a 90° bend upstream of the distributor on the distribution performance for wheat. The distributor, with equal secondary hose lengths, was simulated at three alternate positions (0, 1, and 2 m [0, 3.28, and 6.56 ft]) away from the 90° bend (0.94 m [3.08 ft] radius) at a single fan speed of 3,100 RPM (as displayed in **Figure 10**). The results are discussed below in this section.

The initial distribution performance can be visualized in **Figure 21** and **Figure 22**. The results from the 0 m offset are the most notable with the poorest overall performance. A CV of 67.4% is well below any acceptable range of distribution performance. The airflow CV is also higher than the other configurations. As seen in **Figure 23**, the wheat trajectory continues to follow the path from the 90° bend into the J-tube and dimple tube. Wheat particles can be seen impacting the distributed head closer to the secondary run (7); confirmed with the seed mass fraction in **Figure 21**. **Figure 23** also shows the particles achieving near prebend, steady-state conditions for the 1 and 2 m (3.3 and 6.56 ft) offsets. The 2 m (6.56 ft) offset has the wheat completely exiting the bend trajectory and regaining a standard position in the lower half of the primary tube before entering the J-tube. The particles in the 1 m (3.28 ft) offset appear to just exit the bend trajectory near the outside of the J-tube.

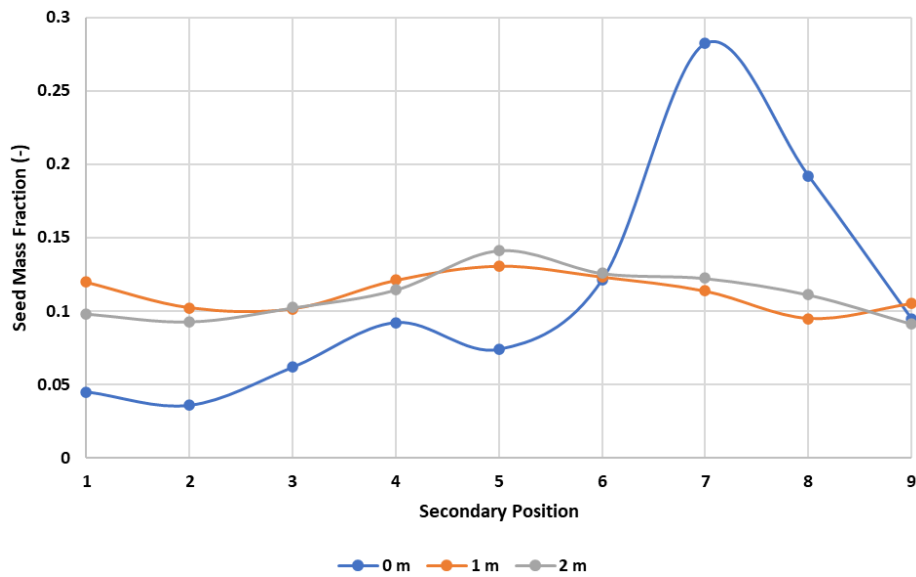


Figure 21. Wheat seed mass fraction through each secondary hoses for the 90° bend into the distributor with equal hoses at three alternate distances (0, 1, and 2 m [0, 3.28, and 6.56 ft]).

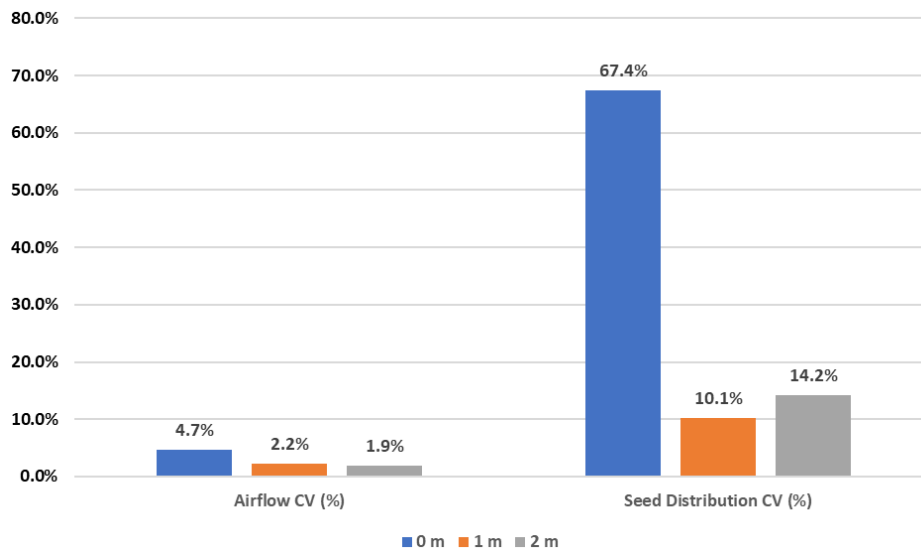


Figure 22. The airflow and seed coefficient of variation for the 90° bend into the distributor with equal hoses at three alternate distances (0, 1, and 2 m [0, 3.28, and 6.56 ft]).

Intuitively, it may be expected for the distribution to improve with a greater offset between the bend and distributor. As identified in **Figure 22**, this is not the case; the 1 and 2 m (3.3 and 6.56 ft) offsets have a CV of 10.1% and 14.2% respectively. **Figure 21** also confirms a more equal distribution for the 1 m (3.28 ft) offset over the 2 m (6.56 ft). To better understand the wheat behavior, more attention should be spent on **Figure 18** and **Figure 24**. The particle velocity and position entering the J-tube appear to affect the distributor CV. The 1 m (3.28 ft) offset, and the 2,800 RPM simulation (idealized distributor with even secondary hoses) have similar CVs and velocities (10.1% - 11.5 m/s [37.7 ft/s] and 11.6% - 11.1 m/s [36.4 ft/s], respectively). A similar trend can be noticed with the 2 m (6.56 ft) offset and 3,400 RPM simulation (14.2% - 13.0 m/s [42.7 ft/s] and 13.3% - 13.9 m/s [45.6 ft/s], respectively).

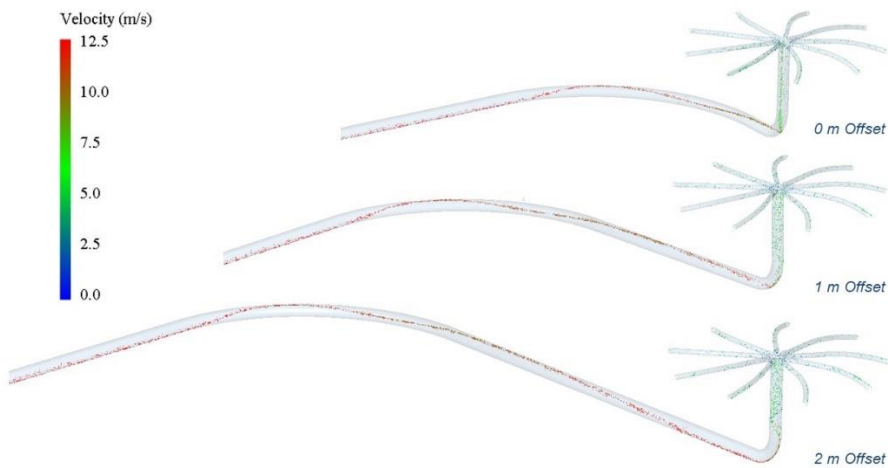


Figure 23. Wheat particle trajectory colored by velocity through the system with equal secondary lengths and three offset distances (simplified geometry for visualization) at 3,100 RPM.

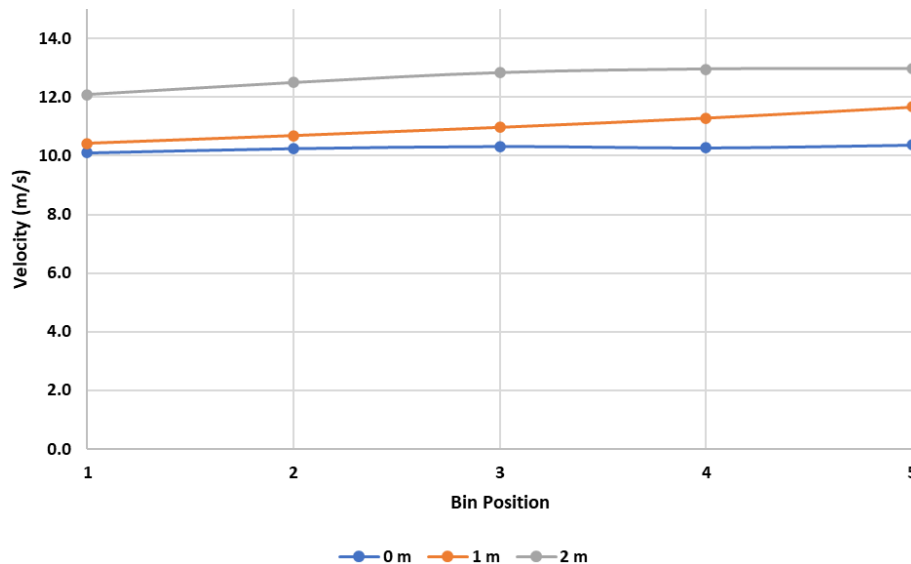


Figure 24. Particle velocity along direction entering the J-tube distributor (left to right – furthest to closest to distributor) for the 90° bend into the distributor with equal hoses at three alternate distances (0, 1, and 2 m [0, 3.28, and 6.56 ft]).

Despite having a constant fan speed of 3,100 RPM for the offset distributor simulations, particles are exiting the 90° bend and reaccelerating at varying points for the different offsets. This variability is affecting the velocity at which particles enter the J-tube. It should also be noted that with the 1 m (3.28 ft) offset simulation, particles are further randomized at the point of impact in the J-tube (**Figure 23**), which resulted in the lowest CV value of all the simulations at 10.1%. This occurrence is indicative of the combined input factors: metering rate, product type, fan speed, bend radius, and distributor offset. This overall behavior highlights the variability in distributor performance when certain input factors are changed.

6. CONCLUSION

The three simulated 90° bends displayed a consistent input velocity before entering the curvature but had varying reacceleration and flow patterns upon exiting. The larger radius bend of 1.24 m (4.07 ft) delayed the wheat product reacceleration and caused a greater disturbance before regaining a prebend flow regime in the bottom half of the hose. Modifying product type, rate, and airflow velocity for a given 90° bend can have a varying result on how the particles regain a steady-state flow regime. The simulated range of bends (0.64 m, 0.94 m, and 1.24 m [2.01, 3.08, and 4.1 ft]) were based on measurements from a physical air drill (JD 1870 drill and 1910 air cart).

For the idealized distributor with equal secondary hoses, the lower fan speed of 2,800 RPM had the lowest CV of 11.6%. Increasing the fan speed also increased the CV value up to 13.3% for the given product rate of 60.14 g/s (60 lb/ac equivalent) of wheat. The operator manual for the John Deere air drill (JD 1870 drill and 1910 air cart) recommended a fan speed range between 2,800 RPM and 3,500 RPM for 50 to 100 lb/ac of wheat at 5 mph (for the given air drill width and single shoot configuration). This highlights the importance of correctly interpreting and adjusting the fan settings for a specific product type and rate.

Secondary runs 5 and 6 consistently had higher seed counts for the idealized distributor at all fan speeds. An equivalent 1 m (3.28 ft) of hose was added to each of these runs for the uneven distributor simulations. This added length was intended to create an additional restriction in the lines and improve the distributor's CV. The airflow CV increased from approximately 2% to 8% while the product CV decreased slightly by 1%. Heavier products such as wheat are less influenced by airflow imbalances. To significantly impact the CV value of the distributor, the required added length to some of the secondary hoses may become impractical for the air drill layout. Regardless, it may still be beneficial to route the longer secondary hoses to outside edge of the J-tube (runs 4 to 7).

A single bend radius of 0.94 m (3.08 ft) was offset at varying distances (0 m, 1 m and 2 m [0, 3.28, and 6.56 ft]) from a distributor with equal secondary hose lengths. These configurations were simulated at a single fan speed of 3,100 RPM and product rate of 60.14 g/s (60 lb/ac equivalent). The worst CV of 67.4% came with the 0 m offset. Wheat was not able to regain a favorable position and velocity prior to entering the J-tube and distributor. A directional bias towards run 7 was apparent and create the dramatic increase in the CV. The 1 m and 2 m (3.28 and 6.56 ft) offsets had significantly lower CVs (10.1% and 14.2%, respectively) that coincided with the performance of the idealized distributors at 2,800 RPM and 3,400 RPM, respectively. Similar particle velocities were achieved between the 1 m (3.28 ft) offset at 3,100 RPM and the idealized distributor at 2,800 RPM. A similar instance occurred with 2 m (6.56 ft) offset at 3,100 RPM and the idealized distributor at 3,400 RPM. This trend outlines the effect of particle velocity on the distribution. It should be noted that the 1 m (3.28 ft) had an even lower CV (10.1%) than the idealized distributor at 2,800 RPM (11.6%). This is due to the particles not fully reaching their prebend, steady-state behavior. Particles were slightly higher in the primary hose

and impacted the J-tube differently causing for a greater randomization and lower resulting CV. These results identify a serious risk when not correctly offsetting an upstream bend before a distributor. Knowing the exact offset distance can prove challenging, as it may vary based on the bend radius itself and other operating conditions. Similar observations about primary hose orientations and distribution CV were identified by Yatskul et al. (2017).

From the simulated configurations and conditions, distribution consistency can be impacted by the following input factors: metering rate, product type, fan speed, bend radius, and distributor offset. Producers should follow manufacturer recommendations for initially setting fan speeds. A static test is also recommended for finer adjustments of the fan speed and distributor.

7. IMPACT ON OPERATIONAL PRACTICES FOR PRODUCERS

This project represented a multi-year effort in measuring air drill distribution performance, both in the laboratory and at full scale, in addition to simulating various configurations of pneumatic conveying systems. While several themes from the results point to opportunities for improved design of these systems, within the confines of existing machines, the project ultimately highlighted the importance of simple but careful maintenance of air drill pneumatic conveying components and systems.

Consistent secondary hose lengths and resulting pressure drops are important to system performance; however, the interaction between secondary hose length and outlet position is complex. Therefore, the manufacturer suggested hose routings should be followed unless actual performance data suggests otherwise. If seed distribution consistency is in doubt, verifying the actual performance of a drill in the range of operation by an operator is a small cost, particularly when weighed against modern input commodity prices.

Wherever possible, severe bends should be minimized in both primary and secondary hoses. Introducing sharp bends close to the entry of a J-tube elbow should be avoided when replacing primary hoses. Ensuring a minimal offset from any bends before the J-tube would also help maintain a consistent coefficient of variation (CV). Furthermore, the hose fastening/restraint schemes suggested by manufacturers should be used. Replace damaged or kinked hoses immediately.

In the range of solids loading ratios (SLRs) tested (relatively low when compared to most other seed and fertilizers) with the equipment studied in this project, increasing the fan speed actually worsened the distribution consistency, as opposed to improving it by “promoting more mixing” as is sometimes anecdotally suggested. In the simulation results, distribution consistency was no better when the air velocity increased. In the testing conducted for this project, the manufacturer-suggested fan speed provided the most consistent distribution of seed across the air drill.

Furthermore, the airflow distribution was generally quite consistent across the range of fan speeds tested for the air drill geometries considered throughout this work. Unless drill-specific information suggests otherwise, the most appropriate fan speed is the one suggested by the manufacturer. If a range of fan speeds is suggested for a broader range of metering rates, special care should be taken when interpreting and setting the fan speed for the specific metering rate.

8. REFERENCES

- Allam, R. K., & Wiens, H. (1982). An investigation of air seeder component characteristics. *1982 Winter Meeting*. Chicago: American Society of Agricultural Engineers.
- Altair Engineering Inc. (2021). EDEM 2021.1. *EDEM User guide*. Troy, Michigan, United States of America.
- Altair Engineering Inc. (2021). HyperWorks CFD 2021.1. *HyperWorks CFD 2021.1 User Guide*. Troy, Michigan, United States of America.
- Bayati, M., & Johnston, C. (2017). *CFD-DEM investigation of seed clustering in an air seeder with the immersed boundary method*. Grand Prairie: Radix Innovation Corporation.
- Bjarnason, T., Stock, W., Hultgreen, G., & Wassermann, J. (2005). *Reducing canola seed damage from metering and air distribution systems*. Humboldt: Prairie Agricultural Machinery Institute.
- Boac, J., Casada, M., Maghirang, R., & Harner III, J. (2010). Material and interaction properties of selected grains and oilseeds for modeling discrete particles. *Transactions of the ASABE*, 1201-1216.
- Bourges, G., & Medina, M. (2013). Air-seeds flow analysis in a distributor head of an "air drill" seeder. *Proceedings 1st international symposium on CFD applications in agriculture* (pp. 259-264). Valencia: International society for horticultural science.
- Bourges, G., Eliach, J. J., & Medina, M. A. (2017). Numerical investigation of a seed distributor head for air seeders. *Chemical Engineering Transactions*, 571-576.
- Bourges, G., Eliach, J., & Medina, M. (2015). Numerical testing of a distributor head modification of an air drill seeder: A performance comparison with actual model. *XXXVI CIOSTA CIGR V Conference*. St. Petersburg: Commission Internationale del'Organisation Scientifique du Travail en Agriculture.
- Chung, C. J. (1969). Mechanical damage to corn in a pneumatic conveying system. Manhattan, Kansas: Kansas State University.
- Cousins, J. D., & Noble, S. D. (2017). Simulation of multiphase flow conditions in air seeders for control applications. *CSBE/SCGAB 2017 Annual Conference* (pp. 1-10). Winnipeg: The Canadian Society for Bioengineering.

- Ebrahimi, M. (2014). *CFD-DEM modelling of two-phase pneumatic conveying with experimental validation*. Edinburgh: Univeristy of Edinburgh.
- Eskin, D., Leonenko, Y., & Vinogradov, O. (2007). An engineering model of dilute polydisperse pneumatic conveying. *Chemical Engineering & Processing*, 247-256.
- Ganser, H. H. (1993). A rational approach to drag prediction of spherical and nonspherical particles. *Powder Technology*, 77(2), 143-152.
- Gieger, L. (2018). *Air seeder distribution and seed damage for wheat, canola, and soybeans*. Portage la Prairie: Prairie Agricultural Machinery Institue.
- Haider , A., & Levenspiel, O. (1989). Drag coefficient and terminal velocity of spherical and nonspherical particles. *Powder Technology*, 58(1), 63-70.
- Hossain, M. S. (2014, December). Development of semi-empirical models to measure mass flow rate of solids in an air seeder. University of Saskatchewan.
- Hubert, M., & Kalman, H. (2003). Experimental determination of length-dependent saltation velocity in dilute flows. *Powder Technology*, 156-166.
- Keep, T. (2016). *Effect of localized velocity increase on overall power consumption and flow characteristics in pneumatic conveying systems*. Saskatoon: University of Saskatchewan.
- Klinzing, G. E., Rizk, F., Marcus, R., & Leung, L. S. (2010). *Pneumatic conveying of solids: A theoretical and practical approach*. Springer.
- Kumar, V., & Durairaj, C. (2000). Infulence of head geometry on the distributive performance of air-assissted seed drills. *Journal of Agriculturan Engineering Research*, 81-95.
- Landry, H. (2018). *Discrete Element Modeling of Porosity Distribution in Grain Bulks (SWDC Ref # 151106-24)*. Humboldt: Prairie Agricultural Machinery Institute.
- Mills, D. (2016). *Pneumatic conveying design guide*.
- Mittal, L. (2016, November). *Identifying the flow conditions in pneumatic conveying of wheat grains through horizontal straight and bent pipe using pressure drop*. Thesis, University of Saskatchewan, Saskatoon. Retrieved December 20, 2022, from <https://harvest.usask.ca/bitstream/handle/10388/7695/MITTAL-THESIS-2016.pdf?isAllowed=y&sequence=1>
- Patwa, A., Ambrose, R., & Casada, M. E. (2016). Discrete element method as an approach to model the wheat milling process. *Powder Technology*, 302, 350-356.
- Paulson, I., Gerspacher, J., & Sprenger, C. (2023). *Pneumatic Grain Conveying in Seeding Equipment*. Humboldt, SK: PAMI (Prairie Agricultural Machinery Institute).
- Paulson, I., Sprenger, C., & Gerspacher, J. (2023). *Pneumatic Grain Conveying in Seeding Equipment*. Prairie Agricultural Machinery Institute, Humboldt.

- Petingco, M. C. (2020). *Discrete element method simulation of wheat bulk density*. Manhattan, Kansas: Kansas State University.
- R Core Team. (2021). R: A language and environment. Vienna, Austria. Retrieved from <https://www.R-project.org/>
- Ratnayake, C. (2017). Pneumatic conveying of wheat flour : system optimisation through pilot testing. *18th International Conference on Transport and Sediment of Solid Particles*, (pp. 257-264). Prague.
- White, F. M. (2006). *Fluid Mechanics*. Mcgraw-Hill College.
- Yatskul, A., Lemiere, J.-P., & Cointault, F. (2017). Influence of the divider head functioning conditions and geometry on the seed's distribution and accuracy of the air-seeder. *Biosystems Engineering*, 120-134.

For further information with regards to this report, please contact:

PAMI@pami.ca



Saskatchewan Test Site

Box 1150
2215 – 8th Avenue
Humboldt, SK S0K 2A0
1-800-567-7264